Received: 11 April 2022 | Revised: 1 August 2022 | Accepted: 7 August 2022

DOI: 10.1002/bio.4368

RESEARCH ARTICLE

LUMINESCENCE The Journal of Biological and Chemical Luminescence WILEY

Development of a mycolic acid-graphene quantum dot probe as a potential tuberculosis biosensor

Kapambwe P. Kabwe | Sifiso A. Nsibande | Lynne A. Pilcher | Patricia B. C. Forbes

Department of Chemistry, Faculty of Natural and Agricultural Sciences, University of Pretoria, Pretoria, South Africa

Correspondence
Patricia B.C. Forbes, Department of Chemistry, Faculty of Natural and Agricultural Sciences, University of Pretoria, Pretoria, South Africa.
Email: patricia.forbes@up.ac.za

Funding information
NRF-TWAS Scholarship, Grant/Award Number: KK; University of Pretoria, Grant/Award Number: N/A

Abstract

The development of amine-functionalized graphene quantum dots (GQDs) linked to mycolic acids (MAs) as a potential fluorescent biosensor to detect tuberculosis (TB) biomarkers is described. GQDs have attractive properties: high fluorescence, excellent biocompatibility, good water solubility, and low toxicity. MAs are lipids that are found in the cell wall of *Mycobacterium tuberculosis* that are antigenic, however, they are soluble only in chloroform and hexane. Chloroform-soluble MAs were covalently linked to synthesized water-soluble GQDs using an amide connection to create a potential fluorescent water-soluble TB biosensor: MA-GQDs. Fluorescence results showed that GQDs had a narrow emission spectrum with the highest emission at 440 nm, while MA-GQDs had a broader spectrum with the highest emission at 470 nm, after exciting at 360 nm. The appearance of the peptide bond (amide linkage) in the Fourier-transform infrared spectrum of MA-GQDs confirmed the successful linking of MAs to GQDs. Powder X-ray diffraction exhibited an increase in the number of peaks for MA-GQDs relative to GQDs, suggesting that linking MAs to GQDs changed the crystal structure thereof. The linked MA-GQDs showed good solubility in water, high fluorescence, and visual flow through a nitrocellulose membrane. These properties are promising for biomedical fluorescence sensing applications.

KEYWORDS
fluorescence, graphene quantum dots, lateral flow, mycolic acid, tuberculosis

1 | INTRODUCTION

Graphene quantum dots (GQDs) are zero-dimensional carbon-based nanocrystals with a diameter between 1 and 20 nm.[1] GQDs have been produced and widely studied in recent years due to their exceptional electronic, optical, and photoelectric attributes including; size-tunable bandgap energy and high surface to volume ratio.[2] Compared to semiconductor-based quantum dots, GQDs possess attractive features such as stable fluorescence properties, simple and cost effective preparation methods, low toxicity, excellent biocompatibility, and good water solubility.[3] As a result of these exceptional attributes, GQD-based materials have been used in biological imaging, biosensing, drug delivery, optoelectrical detectors, solar cells, filtration devices, and photocatalysis.[4–7] Additionally, GQDs have emerged as potential fluorophores for biosensing in biological matrices such as human blood, urine, sputum, and saliva, due to the selectivity, sensitivity, and reproducibility of the results.[8]

Mycolic acids (MAs), also called 2-alkyl-3-hydroxy-long-chain fatty acids, are lipids that are located in the cell walls of *Mycobacterium tuberculosis* (M.tb), the agent that causes the disease tuberculosis (TB).[9] MAs are made up of a long beta-hydroxy chain and a long alpha-alkyl side chain.[10] Depending on the size and nature of the functional groups in the long hydroxy chain, MAs are divided into three main classes, namely alpha-MAs, methoxy-MAs, and keto-MAs.[11] MAs are sometimes referred to as antigenic cell wall lipids because they elicit an antibody response.[12] MAs are strongly

hydrophobic molecules that create a lipid shell over the organism. This affects the permeability properties of the cell surface, hence protecting the organism against lysozymes, oxygen radicals, and cationic proteins.[13]

Anti-MA antibodies serve as specific TB biomarkers that can provide prognostic information about health status and can advance knowledge of disease pathogenesis in predicting reactivation, cure, and induced vaccine protection either for individual patients or study cohorts.[14] Detection of the anti-MA TB biomarker via its association with chemically inert MAs is an attractive proposition. Nevertheless, the insolubility of MAs in bulk solvents apart from chloroform and hexane presents a big challenge to their application as biosensors and in TB diagnosis.[15]

The nitrocellulose membrane lateral flow assay is a technique used in medical diagnostics for point of care testing, laboratory use, and home testing to detect the target analyte, often an antibody in a liquid centered on an antigen–antibody interaction.[16] The nitrocellulose membrane lateral flow assay is typically comprised of four components, namely, the sample pad, conjugate pad, nitrocellulose membrane, and absorbent pad. The sample pad is where the sample is introduced first, acting as a sponge, and holding the sample fluid. The sample fluid is then transported to the conjugate pad through capillary action. The conjugate pad contains the sample and bioconjugate molecules (probe) required for a strong attraction via intermolecular forces between the target molecules to form an immune complex. The reactive area of lateral flow assay is the nitrocellulose membrane, which contains the control and test lines for antigen–antibody interaction. The test line recognizes the sample of interest, while the control line captures unbound conjugate antibodies or antigens from the conjugate pad. The absorbent pad acts as a waste drain and stops the liquid from flowing backwards.[17,18] In this present study, the lateral flow assay strips were composed of three components namely, sample conjugate release pad, nitrocellulose membrane (test pad), and absorbent pad used for a visual flow test.

TB is one of the deadly contagious diseases caused by the M.tb bacterium.[19] Early detection of this disease at the point of care is a serious obstacle worldwide, more especially in less developed countries.[20] The Global Tuberculosis Series 2020 report indicated that about ten million cases of TB were reported in 2020, and about 1.5 million people died from TB.[21] Therefore, this work focuses on progress towards providing a solution to meet the need for facile TB detection. The linking of chloroform-soluble lipid MAs to water-soluble GQDs to provide a water-soluble fluorescent biosensor to detect TB anti-MA antibodies has not been reported previously to the best of our knowledge. The linking of MAs to water-soluble fluorescent GQDs is expected to improve the water solubility of the MAs and thus enable them to be used as a fluorescent TB biosensor. In this study, we present for the first time the linking of chloroform-soluble MAs to water-soluble GQDs to form MA-GQDs and show that this enhances the solubility of MAs, and enables their lateral flow, whilst also reducing the toxicity of the sensor material as compared to semiconductor-based quantum dots, which we have reported on previously.[22]

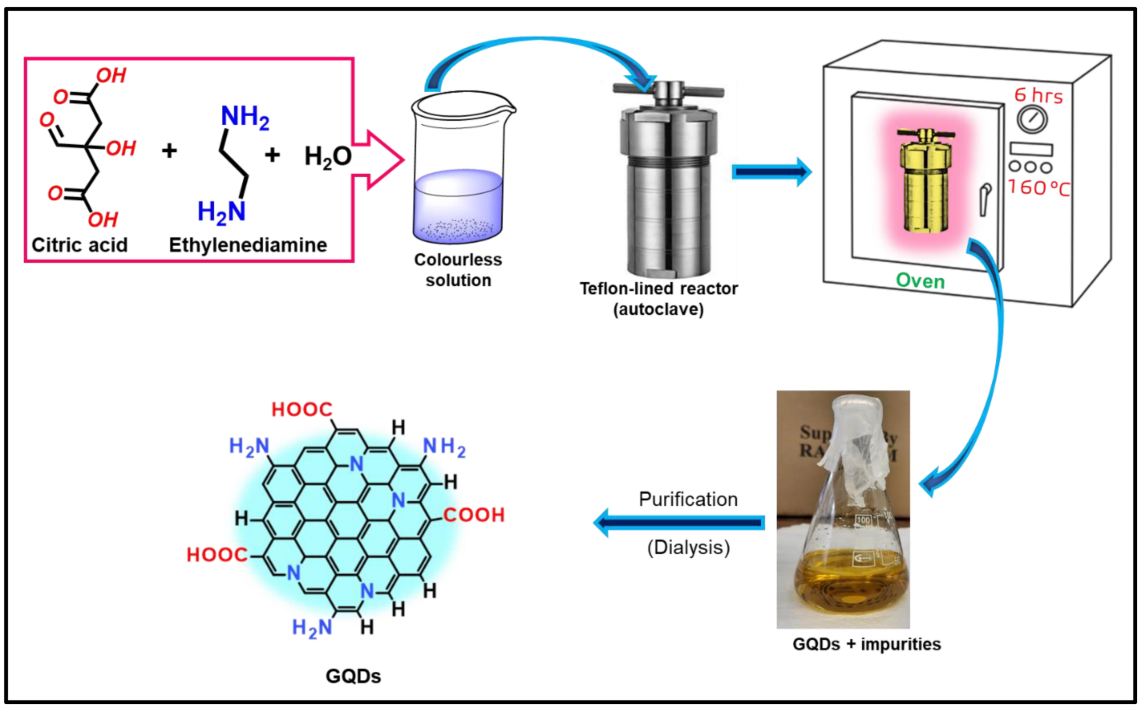

FIGURE 1 Schematic of the hydrothermal synthesis of GQDs from citric acid and ethylenediamine as sources of carbon and nitrogen respectively.

2 | EXPERIMENTAL

2.1 | Materials and reagents

Citric acid (CA, 98%), ethylenediamine (EDA, 99.5%), MA (98%), and oxalyl chloride [$(COCl)_2$, 97.5%] were procured from Sigma-Aldrich (Taufkirchen, Germany) and used as received. The solvents chloroform ($CHCl_3$, 99%), dimethylformamide (DMF, 98.5%), acetone (99.5%), and dichloromethane (DCM, 99.8%) were procured from Associated Chemical Enterprises (Johannesburg, South Africa) and used without further purification. Triethylamine (TEA, 99%), and pyridine (99.5%) were purchased from Radchem Laboratory Chemicals and Consumables (Alberton, South Africa). SnakeSkin dialysis tubing (3.5 kDa MWCO, 22 mm) was procured from Thermo Fisher Scientific (Johannesburg, South Africa) and filter paper (Whatman Macherey-Nagel, 125 mm, MN 615 D) from Altmann Analytik GmbH & Co, Munich, Germany. Deionized (DI) water was acquired using a Drawell water purification laboratory in-house system (Drawell Scientific Instrument Co, Ltd, Greenville, USA) while Argon was provided by African Oxygen Limited (Afrox, Pretoria, South Africa). Nitrocellulose membranes (Sartorius Stedim Biotech, Gottingen, Germany) were provided by the Council for Scientific and Industrial Research (CSIR), Pretoria, South Africa.

2.2 | Instrumentation

The electronic absorption spectra of GQDs and MA-GQDs were obtained using an ultraviolet-visible (UV-vis) Cary Eclipse spectrophotometer (Varian Pty Ltd, Victoria, Australia). Fluorescence was analyzed by a Yvon Jobin Horiba Fluoromax-4 spectrofluorometer (Horiba Instruments Inc., Edison, NJ, USA) at 360 nm excitation, with slit widths set at 5 nm. The infrared investigations were done using a Bruker Alpha (II) spectrometer (Bruker Optik GMBh, Ettlingen, Germany) over 4000–400 cm^{-1} furnished with the Opus software. The morphology and size of the GQDs and MA-GQDs were measured using transmission electron microscopy (TEM) with a JEOL JEM 2100F (JOEL Ltd, Tokyo, Japan), and the software ImageJ was used to analyze the particle size distribution. X-ray diffraction (XRD) spectra were studied using a D2 Bruker phaser (Bruker AXS GmbH, Karlsruhe, Germany) using Cu Kα radiation. The data obtained were collected in the range from $2\theta = 10^{\circ}$ to 90°. A Teflon™ lined stainless steel autoclave (100 mL, 200 °C maximum working temperature) was purchased from Systec, Linden, Germany. Raman spectra were measured using a Horiba T64000 spectrometer (Horiba Jobin Yvon, Palaiseau, France) with a 633 nm laser source operating at 0.5 and an integration time of 3 min.

2.3 | Synthesis of amine functionalized graphene quantum dots (GQDs)

CA (0.022 mol) and EDA (0.022 mol) were mixed and dispersed in 40 ml of DI water in a 100 cm^3 flask, following a reported method.[23–25] The reaction mixture was transferred to a Teflon™ lined stainless-steel autoclave and heated at 150 °C for 6 h. The autoclave was left to cool down to room temperature. The obtained yellowish solution was dialyzed for 3.5 h, after which it was frozen and

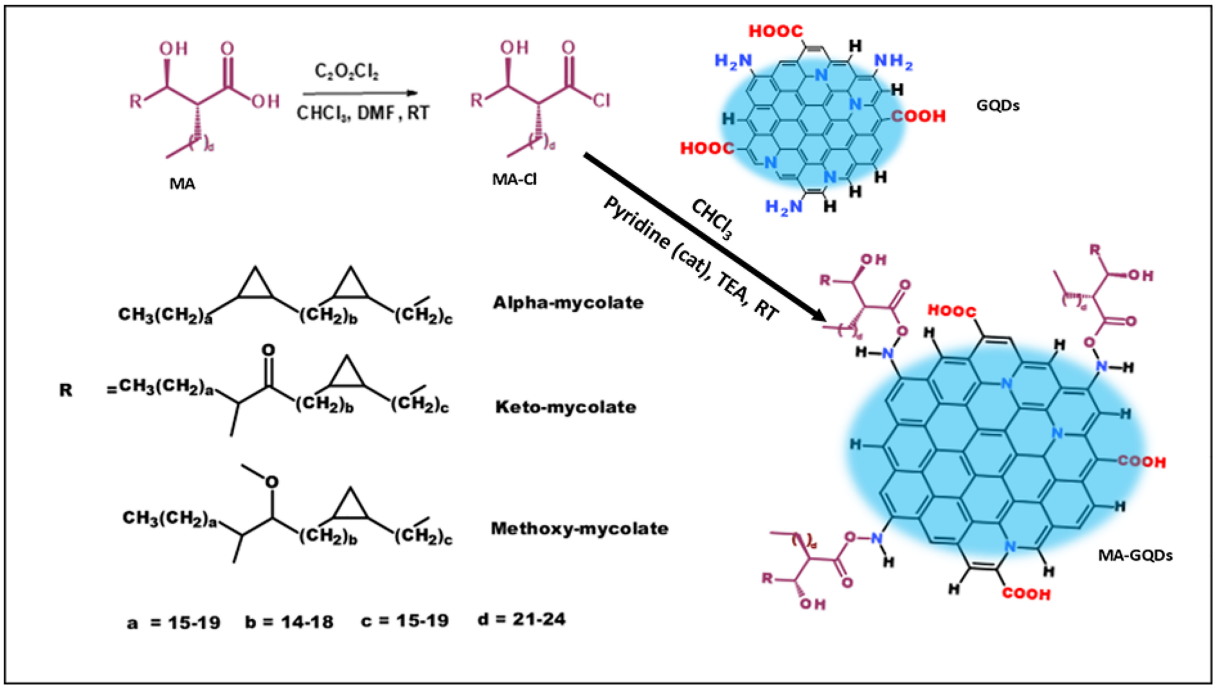

FIGURE 2 Schematic of the covalent linking of chloroform-soluble MAs to water-soluble GQDs to obtain a water-soluble fluorescent TB biosensor: MA-GQDs.

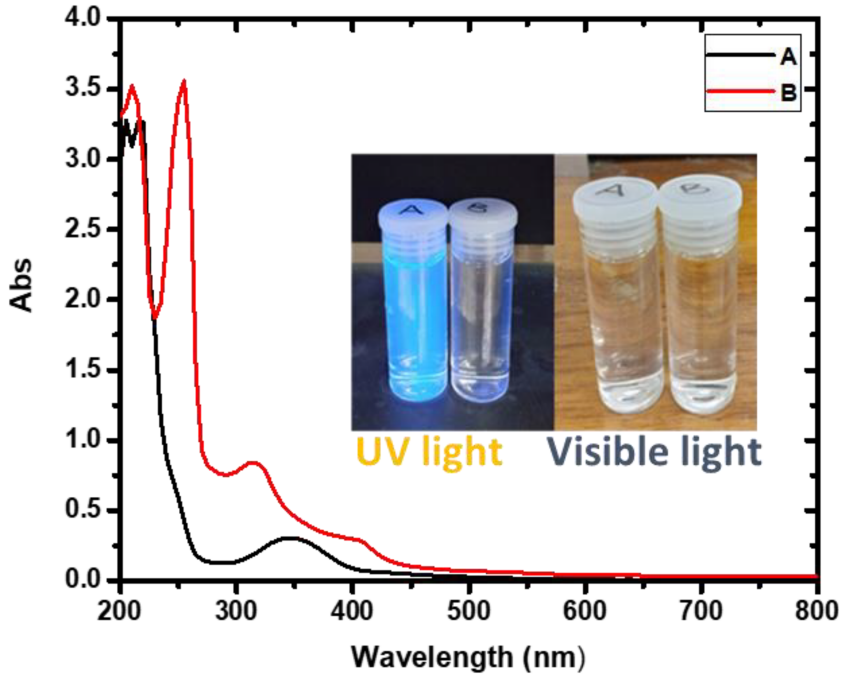

FIGURE 3 UV-vis absorption spectra of GQDs (a) and MA-GQDs (b) dissolved in water (0.01 mg/mL). Insert: GQDs (a) and MA-GQDS (b) under UV light and visible light.

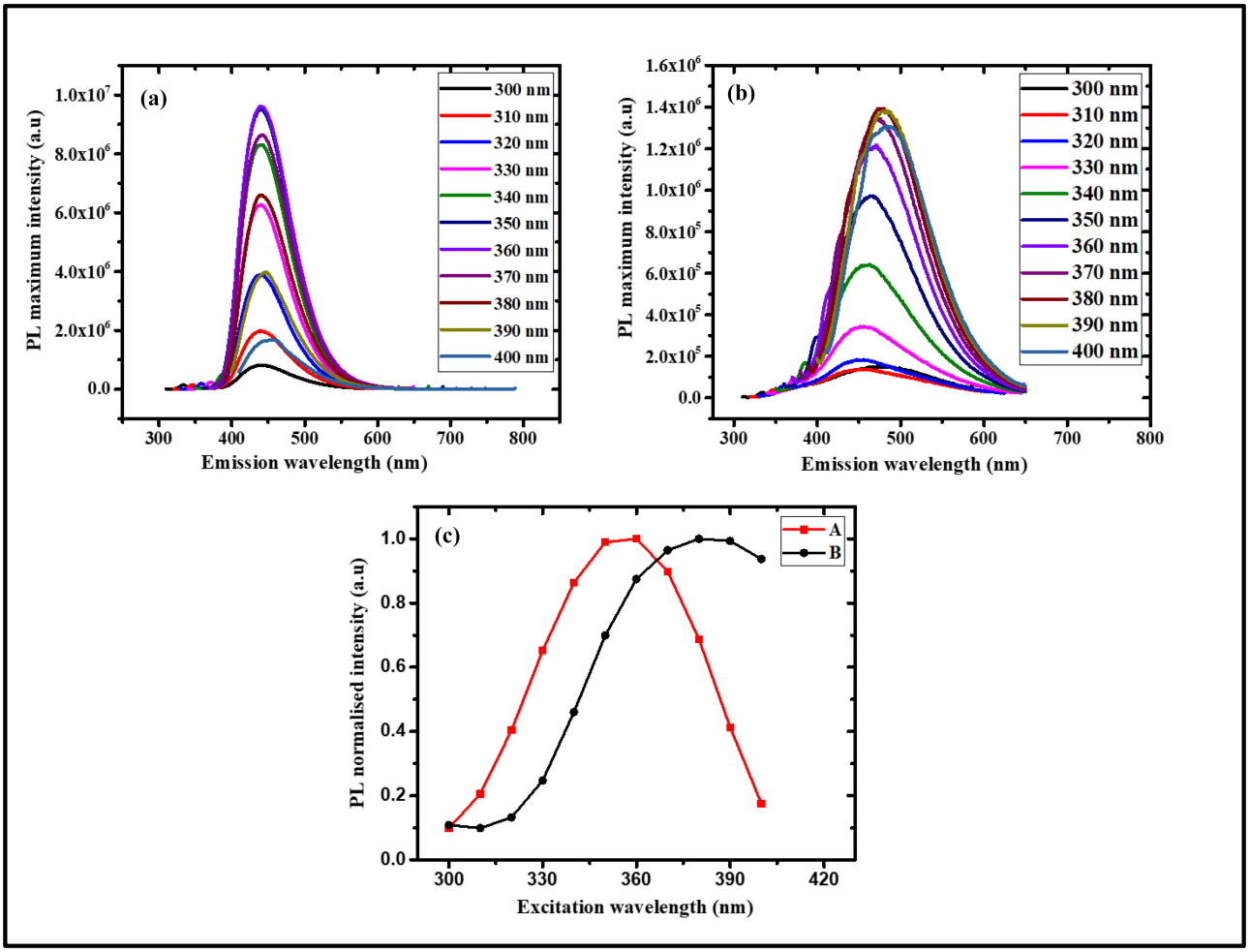

FIGURE 4 Fluorescence spectra of GQDs (a) and MA-GQDs (b) with varying excitation wavelengths. (c) The effect of the excitation wavelength on the maximum photoluminescence (PL) intensity.

then freeze dried for 48 h to obtain yellow crystals of amine functionalized GQDs. A schematic representation of the synthesis is provided in Figure 1.

2.4 | Covalent linking of mycolic acid to amine functionalized graphene quantum dots (GQDs)

Using a round-bottomed flask (50 cm^3), 4.00 mg of MA, 9 cm^3 of dry $CHCl_3$, and DMF (1 drop) were combined. The combination was stirred at 750 rpm for 5 min and soon after, $(COCl)_2$ (1 cm^3) was added with continued stirring at 750 rpm at room temperature for 12 h. Immediately after that, excess $CHCl_3$ was removed via a rotary evaporator to secure a yellow oily mycolic acid chloride, which was then used directly without further purification in the next step.

To link amine-functionalized GQDs to the mycolic acid chloride, 1.50 mg of amine-functionalized GQDs and 9 cm^3 of dry DCM were combined in a round-bottomed flask (100 cm^3). The suspension was purged with argon while stirring for 5 min, and later pyridine (two drops) was added to the suspension as a catalyst. The suspension was placed in a dry ice and acetone bath at the temperature range between 0 °C and −15 °C whilst stirring. Thereafter, mycolic acid chloride was added drop by drop whilst cooling. TEA (five drops) were slowly added to neutralize the acid combination. The reaction mixture was stirred at 750 rpm at room temperature for 12 h and later filtered through filter paper (Whatman Macherey-Nagel, 125 mm, MN 615 D) to remove excess amine-functionalized GQDs. Excess DCM was evaporated under vacuum to secure crystals of mycolic acid-amine functionalized graphene quantum dots (MA-GQDs). A summary of the linking reaction scheme is shown in Figure 2.

2.5 | Calculation of fluorescence quantum yield (Φ_f)

In this study, the fluorescence quantum yield (Φ_f) was calculated using Eqn 1, which used Rhodamine 6G as a standard fluorescence quantum yield (Φ_{std}). The sample fluorescence intensity (I_{sam}) and Rhodamine 6G in ethanol as standard (I_{std}) were compared with the corresponding absorbances of the sample (A_{sam}) and the standard (A_{std}). The refractive index of water for GQDs (n_{sam}) and the refractive index of ethanol for Rhodamine 6G (n_{std}) were used.[26] The absorbances were less

TABLE 1 Summary of fluorescent properties of graphene quantum dots (GQDs) and mycolic acid-amine functionalized graphene quantum dots (MA-GQDs)

	GQDs	MA-GQDs
Wavelength at highest fluorescence emission (λ_{em}, nm)	440	470
Full width at half maximum (FWHM, nm)	57.7	97.2
Fluorescence quantum yield (Φ_f, %)	69.0	21.6

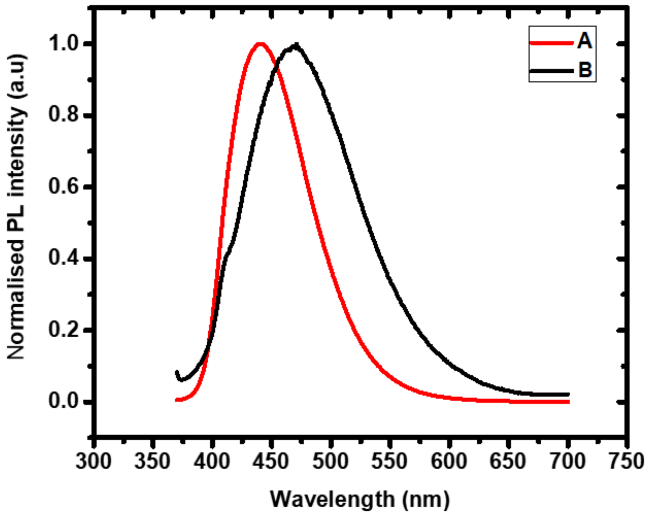

FIGURE 5 Normalized PL emission of GQDs (a) and MA-GQDs (b) dispersed in water when exciting at 360 nm, with slit widths set at 5 nm.

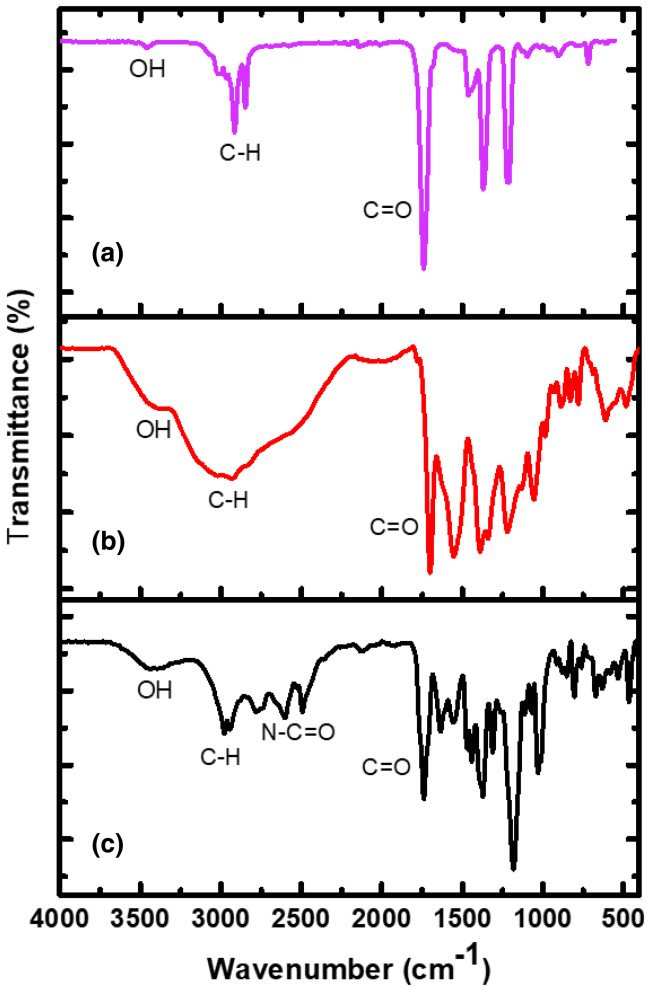

FIGURE 6 FTIR spectra of MAs (a), GQDs (b), and MA-GQDs (c) in solid form.

than 0.05 to minimize internal filter effects, while 360 nm excitation wavelength was used for all the measurements.

$$\Phi_f = \Phi_{std} * \frac{I_{sam} * A_{std} * n^2_{sam}}{I_{std} * A_{sam} * n^2_{std}} \quad (1)$$

2.6 | GQDs and MA-GQDs lateral flow tests

Using 5 cm^3 vials, 0.01 mg/cm^3 solutions of GQDs or MA-GQDs were made, by dispersing 0.01 mg in 1 cm^3 of DI water. Thereafter, 5 μL aliquots of each of the 0.01 mg/mL solution of the GQDs or MA-GQDs were spotted onto 1 cm × 5 cm pieces of nitrocellulose membrane, 5 mm above the bottom edge, using an Eppendorf micropipette. The pieces were dried under ambient laboratory conditions for 1 h and then dipped vertically into individual test tubes holding 200 μL of DI water until the water reached the top part of the membrane strips. A blank piece of the nitrocellulose membrane was similarly eluted as a control. The pieces were removed from the water and dried under ambient laboratory conditions for 2 h. Thereafter, fluorescence analysis was conducted using a Horiba Jobin Yvon Fluoromax-4 spectrofluorometer on two portions of the nitrocellulose membrane strips. The first portion was where the sample was initially deposited (5 mm above the bottom edge), and the second portion was the upper part (5 mm below the upper edge). All the fluorescence spectra were obtained using an excitation wavelength of 360 nm and fluorescence emission was recorded from 370 to 750 nm, with slit widths set at 5 nm.

3 | RESULTS AND DISCUSSION

3.1 | UV-vis absorption properties of GQDs and MA-GQDs

The absorption properties of GQDs and MA-GQDs were explored by UV-vis spectroscopy. The absorption spectra for both GQDs and MA-GQDs exhibit wide absorption bands extending from 200 to

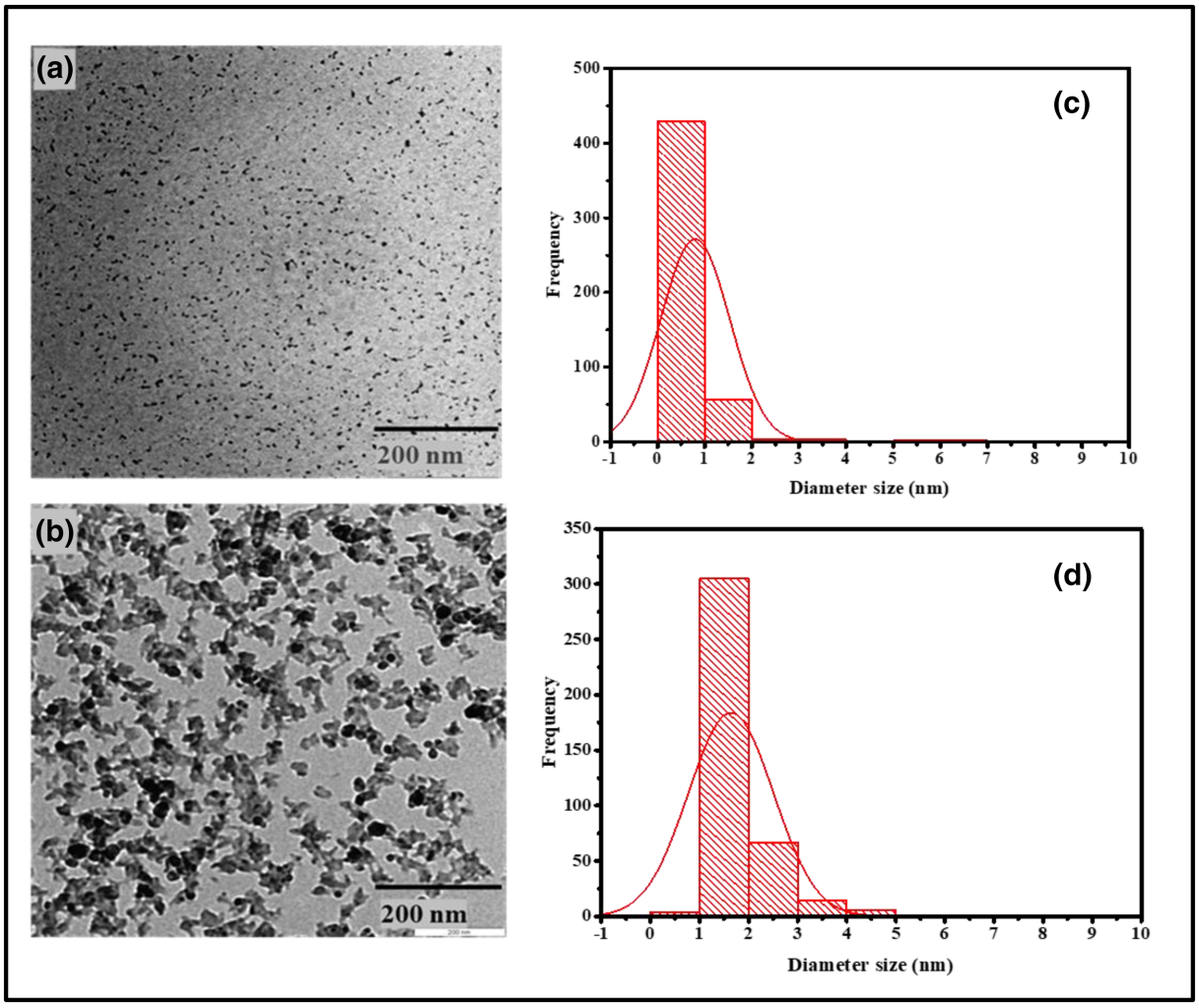

FIGURE 7 TEM micrographs of GQDs (a) and MA-GQDs (b) dispersed in water with the corresponding particle size distribution histograms (c, d).

420 nm with one prominent peak at 344 nm for GQDs, similar to what has been previously reported,[27] while MA-GQDs have prominent peaks at 255, 315, and 408 nm (Figure 3). These wide absorption bands are an excellent property in sensing applications using the fluorescence technique, as they facilitate the use of a range of excitation wavelengths.

3.2 | Fluorescence emission optimization

The optimization of fluorescence emission of GQDs and MA-GQDs were explored by varying the excitation wavelength. It was found that the maximum emission intensity for GQDs was with 360 nm excitation, and 380 nm for MA-GQDs (Figure 4**).** The results also indicated that varying the excitation wavelength did not change the fluorescence emission wavelength of the GQDs, suggesting a pure product with a narrow size distribution. A slight red-shifting was noticed for the emission wavelength of MA-GQDs with an increase in excitation wavelength, which could be due to a variation in the amount of MA coupled to individual GQDs. The fact that the maximum fluorescence emission wavelength of the MA-GQDs did not vary significantly with change in excitation wavelength is evidence for the good purity of the MA-GQDs. The intensity of fluorescence emission of GQDs and MA-GQDs was found to increase to a maximum and thereafter decreased as the wavelength of excitation increased further (Figure 4c).

3.3 | Fluorescent properties of GQDs and MA-GQDs

The fluorescence properties of the synthesized GQDs and MA-GQDs were studied using photoluminescence (PL) spectroscopy (Table 1). The fluorescence emission spectrum of GQDs was narrow, having a full width at half maximum (FWHM) of 57.67 nm with the highest emission wavelength at 440 nm and a fluorescence quantum yield of 69.0% when exciting at 360 nm (Figure 5). Upon the linking of MA to GQDs, the fluorescence quantum yield decreased to 21.6% while the emission spectrum became somewhat broader (FWHM of 97.17 nm) than that of the GQDs and was moderately red shifted with the highest fluorescence emission wavelength at 470 nm. This decrease in the fluorescence quantum yield and the red shift may be attributed to the change in the size and surface properties of MA-GQDs, suggesting the successful linking of MA to the GQDs. The fluorescence quantum yield of the GQDs and MA-GQDs is somewhat lower than the fluorescence quantum yield of semiconductor-based quantum dots and the corresponding MA-QDs reported in our previous work.[22]

3.4 | FTIR analysis of MA, GQDs and MA-GQDs

Figure 6 shows the Fourier-transform infrared (FTIR) spectra of MAs, GQD, and MA-GQDs. The spectra of MAs and GQDs indicate expected characteristic peaks resulting from the presence of –C–H; –OH and –C=O functional groups. The additional peaks between 2450 cm^{-1} and 2790 cm^{-1} in MA-GQDs can be due to –N–C=O modes. The presence of these peaks in MA-GQDs indicates the appearance of the peptide bond, which confirms the covalent linking of GQDs to MAs.

3.5 | TEM analysis of GQDs and MA-GQDs

The particle size and morphology of GQDs and MA-GQDs are shown in Figure 7. It was noticed that GQDs distributed well in water with a mean approximate particle size of 0.8 ± 0.3 nm while the MA-GQDs showed some particle aggregation with a mean approximate particle size of 1.6 ± 0.8 nm. The aggregation observed could be a result of interactions between hydrophobic and hydrophilic groups in the linked MA-GQDs, respectively.

3.6 | Powder XRD study of GQDs and MA-GQDs

The XRD spectrum in Figure 8(a) exhibits one broad peak for GQDs at 20.8° corresponding to the structure reported previously.[23,28,29] The

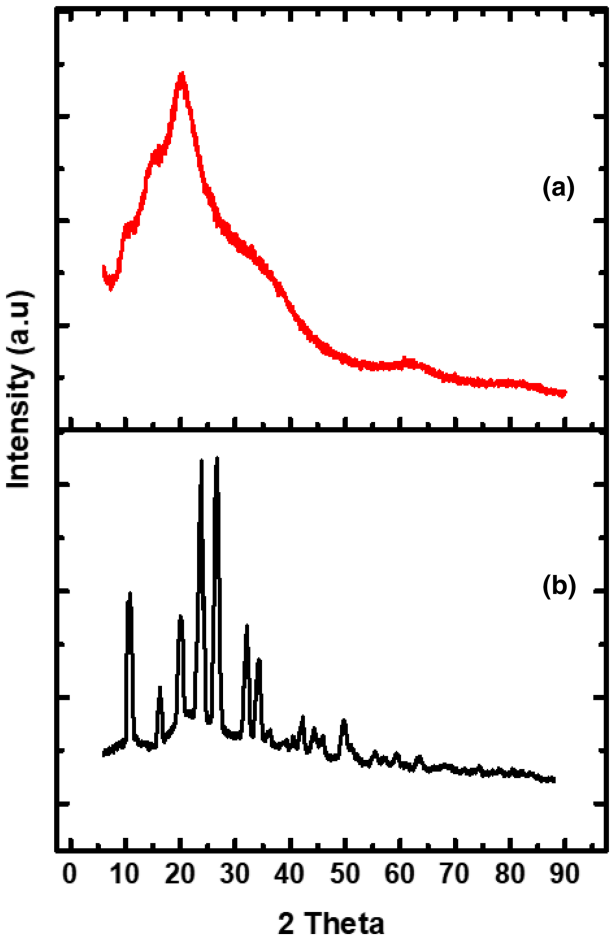

FIGURE 8 Powder XRD spectra of GQDs (A) and MA-GQDs (B).

XRD spectrum of MA-GQDs (Figure 8b) however was clearly different, having ten sharp peaks at positions 12.8°, 18.4°, 22.0°, 25.6°, 28.6°, 33.6°, 36.1°, 44.2°, 46.1°and 51.9°.

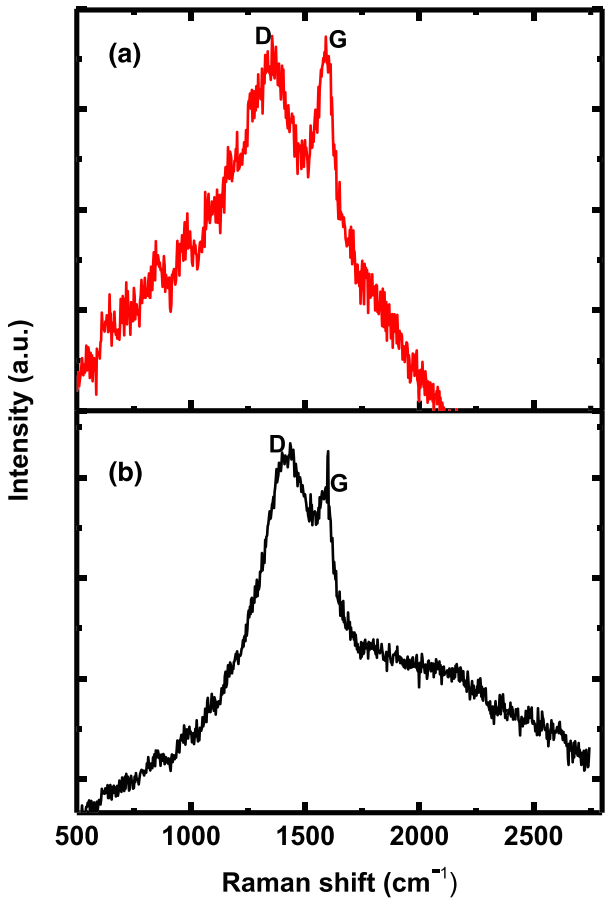

FIGURE 9 Raman spectra of GQDs (a) and MA-GQDs (b)

3.7 | Raman spectra of GQDs and MA-GQDs

The Raman spectra of GQDs and MA-GQDs are shown in Figure 9. The GQD spectrum reveals the presence of the characteristic D and G bands at 1365 cm^{-1} and 1597 cm^{-1} respectively, comparable to what has been previously reported,[30] while the spectrum of MA-GQDs shows the D and G bands at 1428 cm^{-1} and 1597 cm^{-1} respectively. The Raman spectrum of MA-GQDs indicated a red-shift of the D band and decrease in intensity of G band, which may be a result of the changes in the surface chemistry of the materials affecting the interaction of the photons. The ratio of the intensities of the D and G bands (I_D/I_G) for GQDs was 0.85 and 0.89 for MA-GQDs, which confirm the presence of defects in the graphitic structure of the GQDs and MA-GQDs.[31]

3.8 | Lateral flow tests of GQDs and MA-GQDs

The lateral flow of GQDs and MA-GQDs was investigated to determine the possible application thereof in the detection of TB biomarkers which are anti-MA antibodies. Figure 10 shows that GQDs and MA-GQDs were able to flow through the strips of nitrocellulose membrane when using DI water as eluent. This flow of GQDs and MA-GQDs was confirmed by the fluorescence emission spectra obtained at 437 and 430 nm, respectively, when the nitrocellulose membrane was excited at 360 nm. The emission spectra of GQDs (435 nm) and MA-GQDs (450 nm) before lateral flow (i.e. at the point where the sample was deposited onto the strip) were also obtained. The intensity of the emission spectra of GQDs and MA-GQDs after the lateral flow was somewhat lower than before the lateral flow. This is expected, as the GQD and MA-GQD particles are dispersed over a wider area after elution. These results show that GQDs and MA-GQDs are water-dispersible materials that can flow through a lateral

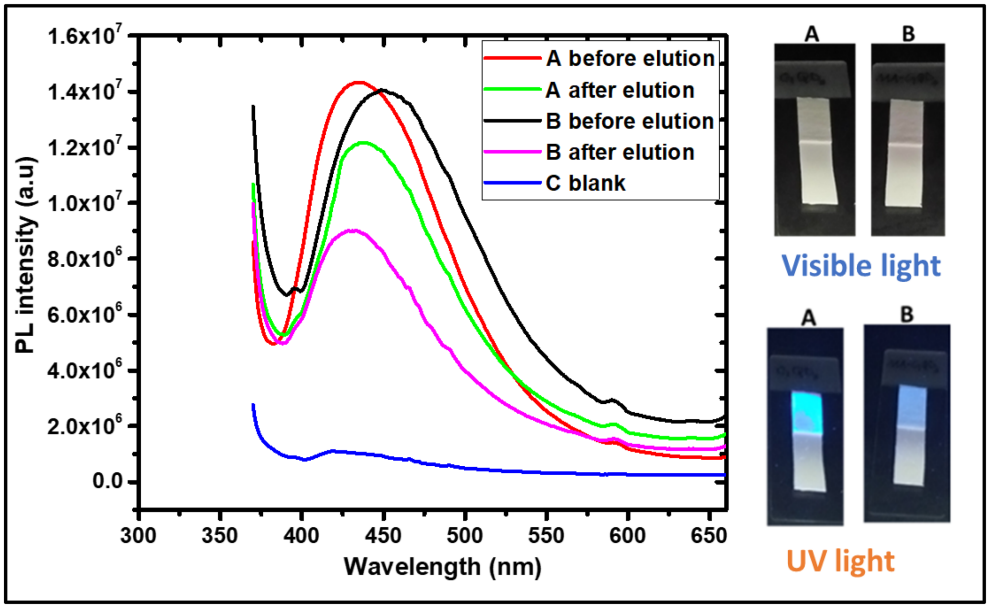

FIGURE 10 PL fluorescence spectra of GQDs (a) and MA-GQDs (b) dried on nitrocellulose membrane strips before elution (5 mm above the bottom edge) and after elution (5 mm below the upper edge). The excitation wavelength used was 360 nm. The inset shows GQDs (a) and MA-GQDS (b) under visible light and UV light after lateral flow.

flow test membrane, and thus MA-GQDs have the potential to detect anti-MA antibodies via the nitrocellulose membrane flow technique. It can be deduced that the MA-GQDs were more dispersible in water as compared to the coupled material prepared with semiconductor quantum dots reported in our previous work.[22] As can be seen in the inset shown in Figure 10, all the sample at the spotting point eluted up the strip, while for the semiconductor based MA-QDs, some spotted sample remained at the initial spotting point. Good solubility in water and low toxicity thus makes MA-GQDs the preferred material to potentially detect anti-MA antibodies and diagnosis of TB using the nitrocellulose membrane flow technique.

4 | CONCLUSION

GQDs were synthesized using a well-established hydrothermal method and were successfully linked to MAs to form MA-GQDs. The synthesized GQDs and linked MA-GQDs were characterized by fluorescence, UV-vis, FTIR, XRD spectroscopy, and TEM analysis. The absorption results showed that both GQDs and MA-GQDs exhibit a wide range of absorption wavelengths between 420 and 200 nm, which enables changes of excitation wavelength used in fluorescence sensing applications. Fluorescence results showed that GQDs have a narrow emission spectrum (FWHM of 57.7 nm), with a fluorescence quantum yield of 69.0% with the highest fluorescence emission wavelength at 440 nm, while MA-GQDs have a somewhat broader spectrum (FWHM of 97.2 nm) and the highest emission wavelength at 470 nm after exciting at 360 nm, with a fluorescence quantum yield of 21.6%. The appearance of –N–C=O peaks between 2450 and 2790 cm^{-1} in the FTIR spectrum of the MA-GQDs indicates the appearance of the peptide bond (amide linkage), which confirms the covalent linking of MAs to GQDs. TEM results exhibited an average approximate particle size distribution of GQDs of 0.8 ± 0.3 nm and 1.6 ± 0.8 nm for MA-GQDs. The powder XRD results showed an increment in the number of peaks for MA-GQDs compared to one broad peak for GQDs. This suggests that the covalent linking of MAs to GQDs changed the crystal structure of the resulting material. Nitrocellulose membrane lateral flow experiments confirmed the elution of MA-GQDs with DI water as eluent.

In view of the simplicity of the process, low toxicity of the material, as well as the good dispersibility of the highly fluorescent MA-GQDs in water, enabling their lateral flow through a nitrocellulose membrane, the novel MA-GQDs have the potential to be used in the detection of anti-MA antibodies and in point of care TB diagnosis. The potential limit of detection of the proposed biosensor will need to be determined to further evaluate the feasibility of application. The use of GQDs in this study showed some competitive advantages over our previous work, where cadmium-based quantum dots were used as a proof of concept for the development of a MA-coupled quantum dot sensor. The use of GQDs has not only averted the potential toxicity concerns of cadmium, but also resulted in improved dispersibility in water which makes it ideal for lateral flow experiments. This study paves the way towards a simple, quick, and cost-effective method for TB detection.

ACKNOWLEDGMENTS

Funding for this work was provided by NRF-TWAS scholarship and a postgraduate student bursary from the University of Pretoria (KK). The authors thank the Microanalysis and Microscopy Laboratory of the University of Pretoria for their help with TEM analysis.

CONFLICT OF INTEREST

The authors declare no conflict of interest.

DATA AVAILABILITY STATEMENT

Data is available upon request.

ORCID

Patricia B. C. Forbes https://orcid.org/0000-0003-3453-9162

REFERENCES

[1] Y. R. Kumar, K. Deshmukh, K. K. Sadasivuni, S. K. Pasha, *RSC Adv.* **2020**, *10*, 23861.
[2] C. Zhao, X. Song, Y. Liu, Y. Fu, L. Ye, N. Wang, F. Wang, L. Li, M. Mohammadniaei, M. Zhang, *J. Nanobiotechnol.* **2020**, *18*, 1.
[3] P. Tian, L. Tang, K. Teng, S. Lau, *Mater. Today Chem.* **2018**, *10*, 221.
[4] W. Chen, G. Lv, W. Hu, D. Li, S. Chen, Z. Dai, *Nanotechnol. Rev.* **2018**, *7*, 157.
[5] L. N. Dinh, L. N. Ramana, V. Agarwal, P. B. Zetterlund, *Polym. Chem.* **2020**, *11*, 3217.
[6] F. Xi, J. Zhao, C. Shen, J. He, J. Chen, Y. Yan, K. Li, J. Liu, P. Chen, *Carbon* **2019**, *153*, 127.
[7] L. N. Dinh, L. N. Ramana, R. P. Kuchel, V. Agarwal, P. B. Zetterlund, *Polym. Chem.* **2020**, *11*, 5790.
[8] B. D. Mansuriya, Z. Altintas, *Sensors* **2020**, *20*, 1072.
[9] E. J. North, M. Jackson, R. E. Lee, *Curr. Pharm. Des.* **2014**, *20*, 4357.
[10] J. Madacki, F. Laval, A. Grzegorzewicz, A. Lemassu, M. Záhorszká, M. Arand, M. McNeil, M. Daffé, M. Jackson, M.-A. Lanéelle, *J. Biol. Chem.* **2018**, *293*, 5172.
[11] M. Beukesa, Y. Lemmera, M. Deysela, J. A. R. Al Dulayymid, M. S. Bairdd, G. Kozad, M. M. Iglesiasd, R. R. Rowlesd, C. Theunissend, J. Grootene, *Chem. Phys. Lipids* **2011**, *163*, 1800.
[12] F. L. Ndlandla, V. Ejoh, A. C. Stoltz, B. Naicker, A. D. Cromarty, S. van Wyngaardt, M. Khati, L. S. Rotherham, Y. Lemmer, J. Niebuhr, C. R. Baumeister, J. R. Al Dulayymi, H. Swai, M. S. Baird, J. A. Verschoor, *J. Immunol. Methods* **2016**, *435*, 50.
[13] M. Watanabe, Y. Aoyagi, M. Ridell, D. E. Minnikin, *Microbiology* **2001**, *147*, 1825.
[14] Y. Lemmer, L. Kalombo, R.-D. Pietersen, A. T. Jones, B. Semete-Makokotlela, S. Van Wyngaardt, B. Ramalapa, A. C. Stoltz, B. Baker, J. A. Verschoor, *J. Control. Release* **2015**, *211*, 94.
[15] S. Shang, D. Kats, L. Cao, E. Morgun, D. Velluto, Y. He, Q. Xu, C.-R. Wang, E. A. Scott, *Front. Immunol.* **2018**, *9*, 2709.
[16] E. B. Bahadır, M. K. Sezgintürk, *TrAC-Trends Anal. Chem.* **2016**, *82*, 286.
[17] L. Anfossi, F. Di Nardo, S. Cavalera, C. Giovannoli, G. Spano, E. S. Speranskaya, I. Y. Goryacheva, C. Baggiani, *Microchim. Acta* **2018**, *185*, 94.
[18] M. Sajid, A.-N. Kawde, M. Daud, *J. Saudi Chem. Soc.* **2015**, *19*, 689.
[19] N. Ariffin, N. A. Yusof, J. Abdullah, S. F. Abd Rahman, N. H. Ahmad Raston, N. Kusnin, S. Suraiya, *J. Sens.* **2020**, *2020*, 1.
[20] S. Sudha, *Int. J. Med. Eng. Inform.* **2016**, *8*, 27.
[21] D. R. Silva, F. C. D. Q. Mello, G. B. Migliori, *J. Bras. Pneumol.* **2020**, *46*, 1806.
[22] K. P. Kabwe, S. A. Nsibande, Y. Lemmer, L. A. Pilcher, P. B. C. Forbes, *Luminescence* **2022**, *37*(2), 278.

[23] H. Safardoust-Hojaghan, M. Salavati-Niasari, O. Amiri, M. Hassanpour, *J. Mol. Liq.* **2017**, *241*, 1114.
[24] L. Wang, W. Li, L. Yin, Y. Liu, H. Guo, J. Lai, Y. Han, G. Li, M. Li, J. Zhang, *Sci. Adv.* **2020**, *6*, eabb6772.
[25] D. Song, H. Guo, K. Huang, H. Zhang, J. Chen, L. Wang, C. Lian, Y. Wang, *Mater. Today* **2022**, *54*, 42.
[26] D. Magde, R. Wong, P. G. Seybold, *Photochem. Photobiol.* **2002**, *75*, 327.
[27] L. Wang, M. Li, Y. Li, B. Wu, H. Chen, R. Wang, T. Xu, H. Guo, W. Li, J. Joyner, *Carbon* **2021**, *180*, 48.
[28] Y. Han, B. Tang, L. Wang, H. Bao, Y. Lu, C. Guan, L. Zhang, M. Le, Z. Liu, M. Wu, *ACS Nano* **2020**, *14*, 14761.
[29] L. Zhang, M. Wu, Z. Wang, H. Guo, L. Wang, M. Wu, *ACS Sustain. Chem. Eng.* **2021**, *9*, 16262.
[30] L. N. Ramana, L. N. Dinh, V. Agarwal, *Nanoscale Adv.* **2021**, *3*, 3513.
[31] S. A. Nsibande, P. B. Forbes, *RSC Adv.* **2020**, *10*, 12119.

How to cite this article: K. P. Kabwe, S. A. Nsibande, L. A. Pilcher, P. B. C. Forbes, *Luminescence* **2022**, *37*(11), 1881. https://doi.org/10.1002/bio.4368